CHAPTER IV

SINGLE STEP COUPLING FOR MULTI-RESPONSIVE WATER-BASED CHITIN/CHITOSAN MAGNETIC NANOPARTICLES

4.1 Abstract

Coupling of chitin whisker (CTWK) or water soluble chitosan (WSCS) with magnetic nanoparticles (MAG) via a covalent linkage by using a silane coupling agent in an aqueous system is proposed. The use of the silane coupling agent glycidoxypropyltrimethoxy, having a trimethoxy silane as well as an epoxide functionality, allows one step coupling between CTWK or WSCS and MAG. The MAG derivatives obtained are well dispersed and their colloidal aqueous solutions can be stabilized for days. An external magnetic field initiates alignment of nano-rod structured CTWK-MAG in the direction of the magnetic field. The uniqueness of these two materials is that CTWK-MAG shows solvent polarity responsiveness whereas WSCS-MAG performs pH responsiveness. A model application study on DNA extraction confirms that WSCS-MAG with positively charged at pH 7 and with high surface area performs more *E.coli* extraction ability for two times as compared to CTWK-MAG.

Keywords: chitin whisker; water-soluble chitosan; magnetic nanoparticles; covalent bond; coupling reaction; DNA extraction

4.2 Introduction

Ferrous oxide in the form of magnetic nanoparticles (MAG) is accepted as an important inorganic functional material. One of the most unique properties of MAG is its superparamagnetism which provides responsiveness to a magnetic field, especially when the particle sizes are less than 15 nm (Gupta and Gupta, 2005). Due to the nanometer size of the particles, the tendency of aggregation is always a problem for applications. In current years, many approaches to overcome this limitation have been proposed by coating with surfactants (Jing and Wu, 2004; Bica *et al.*, 2007; Loo *et al.*, 2008; Xie *et al.*, 2008; Zargar *et al.*, 2009), fatty acids (Richardson *et al.*, 1999; Tadmor *et al.*, 2000), or by encapsulating in polymers. The investigated polymers are poly(vinyl alcohol) (Lao and Ramanujan, 2004; Kim *et al.*, 2012), poly(2-methoxyethyl methacrylate) (Gelbrich *et al.*, 2006), poly(ethylene oxide) and/ or poly(propylene oxide)-grafted-poly(acrylic acid) (Moeser *et al.*, 2002). Coating a MAG surface not only prevents particles from aggregation but also provides specific properties to MAG. Currently, MAG for biomedical applications such as a contrast agent for MRI (Xie *et al.*, 2008), target drug delivery (Zhang *et al.*, 2007), hyperthermia cancer treatment agent (Lao and Ramanujan, 2004), and DNA/RNA or cell separation (Scarberry *et al.*, 2008) have received much attention.

Chitosan, which is the second-most abundant naturally occurring amino polysaccharide offering high biocompatibility (Muzzarelli *et al.*, 2012), up to present, has attracted intense attention as an important biopolymer to functionalize MAG. Several reports have shown MAG coupled to chitosan via secondary forces. For example, Xia *et al.* produced a one-step suspension to cover MAG with carboxymethyl chitosan (Xia *et al.*, 2006). In order to maintain suspension stability of MAG with chitosan, the covalent linkage is more stable compared to the secondary forces. The use of silane reagents is one of the most practical approaches to form covalent linkage between inorganic materials, such as silica, glass fibers, etc., with polymers. De Palma *et al.* showed that covering MAG with hydrophobic molecules, especially oleic acid, followed by a ligand exchange with an alkoxysilane coupling agent, which provides different end groups was a good strategy to modify the MAG surface with organic species (De Palma *et al.*, 2007). López-Cruz *et al.*

reported that the coupling reaction between oleic acid coated MAG (O-MAG) and carboxylic acid silane followed by carbodiimide conjugation with chitosan yielded a covalent bonded MAG and chitosan (Lopez-Cruz *et al.*, 2009). Hu *et al.* reported the success of chitosan coated silica surface by using glycidoxypropyltrimethoxy silane (GPTMS) (Hu *et al.*, 2011).

Chitin and chitosan are good candidate biopolymers for MAG coating, however, a few reports related to study chitin in aqueous solution (Hu *et al.*, 2011). The fact that chitosan is insoluble in organic solvents except mineral acids and carboxylic acids, the reaction conditions in water and avoid the use of organic solvents are still needed. Currently, our group reported good solubility of chitosan in water via complexation with hydroxybenzotriazole (HOBt) to yield chitosan aqueous solution, hereinafter, so-called water-soluble chitosan (WSCS). This modification allows effective conjugating reactions in aqueous solution under mild conditions (Pangkangwanwong *et al.*, 2006). In a separate work, we also succeeded in the preparation of nano-sized chitin whiskers (CTWK) and chitosan whiskers or chitosan nanoscaffolds which are stable in water to give colloidal aqueous solution (Phongying *et al.*, 2007).

As the present work aims to develop MAG conjugated with chitin and chitosan, the key points needed to be considered are, (i) how the reaction can be carried out without the use of organic solvent but water, (ii) how to simplify the steps of preparation and achieve the good product yield, (iii) how MAG coated with chitin or chitosan can be stabilized aggregation, and (iv) if possible, how to develop external stimuli responsive properties to the material.

To satisfy the points above, the materials are the water-based CTWK and WSCS, the reaction in consideration is a single-step coupling reaction by the use of epoxy silane, i.e. GPTMS, to initiate covalent bond between MAG and CTWK, and MAG and WSCS without any use of conjugating agent, whereas the external stimuli responsiveness is expected to obtain based on the performance of the nano-rod morphology of CTWK and the amino group of WSCS. In order to show the potential application of MAG materials obtained, the work extends to a preliminary study on DNA extraction, which relies on the specific properties of MAG, CTWK, and WSCS.

4.3 Experimental

4.3.1 Materials

Chitosan (95% DD, M_w of 7.0×10^5) was the product of Seafresh Chitosan (Lab) Co., Ltd., Thailand. 1-Hydroxybenzotriazole monohydrate (HOBt) was purchased from Tokyo Chemical Industry Co., Ltd., Japan. Iron (II) sulfate hexahydrate (99%) and Iron(III) chloride heptahydrate (98%) were purchased from BDH chemicals, UK. Oleic acid was purchased from Sigma Aldrich Inc., USA. 3-Glycidoxypropyltrimethoxy silane (GPTMS) was bought from Dow Corning Toray Co., Ltd., Japan. Sodium hydroxide was bought from Carlo Erba Reagent, Italy. Tetrahydrofuran (THF), toluene, chloroform, hexane, and ethanol were purchased from Lab-Scan, Ireland. Sodium ethoxide was prepared by dissolving NaOH (0.08 g) in dried ethanol (20 mL) to get a concentration of 0.1 mol L^{-1}. All chemicals were used without further purification.

4.3.2 Preparation of Oleic Acid-Coated MAG (O-MAG)

$FeCl_2 \cdot 4H_2O$ (9.94 g, 0.05 mol) and $FeCl_3 \cdot 6H_2O$ (27.03 g, 0.10 mol) were mixed and stirred in distilled, de-ionized, and de-oxygenated water (200 mL) under N_2 atmosphere for 30 min. Oleic acid (20 mL) was gradually added and the mixture was heated at 50 °C for 15 min. Ammonia solution was further injected via septum until pH 10 to pH 11 and the mixture was heated to 80 °C for 30 min. The precipitates were washed in a dialysis tube (MW cut-off 12000 Da) against de-ionized water until no ammonia was detected. Finally, water was removed from the oleic acid-coated MAG (O-MAG) by freeze-drying.

FTIR (KBr, ν cm^{-1}): 2922, and 2851 cm^{-1} (C-H stretching), 594 cm^{-1} (Fe-O).

4.3.3 Surface Modified MAG with 3-Glycidoxypropyltrimethoxy Silane (S-MAG)

O-MAG (0.3 g) was dispersed in toluene (50 mL) under N_2 atmosphere at 60 °C for 30 min. A catalytic amount of glacial acetic acid was added to the solution before adding GPTMS (1.4 mL). The mixture was stirred for 72 h

followed by precipitating in ethanol and intense washing with ethanol and THF. The precipitates were collected by a strong magnet and dried at 60 °C several hours to obtain black-brown particles.

FTIR (KBr, ν cm^{-1}): 2919, and 2846 cm^{-1} (C-H stretching), 1087 cm^{-1} (Si-O), 900 cm^{-1} (oxirane ring), 588 cm^{-1} (Fe-O).

4.3.4 Preparation of Chitin Whisker - MAG (CTWK-MAG) (Scheme I)

Chitin whisker (CTWK) was prepared as reported previously (Phongying *et al.*, 2007). In brief, chitin (1.0 g) was vigorously stirred with 3 N hydrochloric acid (100 mL) at 105 °C for 3 h. The colloidal solution obtained was then collected and the residues were treated with hydrochloric acid for two times. The residues were then dialyzed until neutral. The CTWK obtained was kept in aqueous solution and the concentration was evaluated by TGA technique. CTWK (0.2 g, 0.001 mol) was dispersed in water (20 mL). A catalytic amount of sodium ethoxide was added into the CTWK suspension at room temperature in a closed stirring system. S-MAG (0.6 g) was added and stirred for 24 h. The colloidal solution was washed several times and the prior precipitates were collected at the bottom by using a strong magnet before decanting the colloidal solution. After excluding the prior precipitates, the strong magnet was applied to collect the colloidal particles followed by rinsing in water for three more times. At final, the particles were collected by a strong magnet and freeze-dried to obtain CTWK-MAG.

CTWK-MAG: FTIR (KBr, ν cm^{-1}): 2921, and 2879 cm^{-1} (C-H stretching), 1661, 1627, and 1563 cm^{-1} (amide I and II), 578 cm^{-1} (Fe-O).

4.3.5 Preparation of Water Soluble Chitosan Coated MAG (WSCS-MAG) (Scheme I)

Chitosan (1.0 g, 0.006 mol) was dissolved in water (100 mL) containing an equivalent mole of HOBt (0.0828 g, 0.006 mol) to obtain water soluble chitosan (WSCS) as reported previously (Fangkangwanwong *et al.*, 2006). The solution obtained (20 mL) was reacted with S-MAG (0.6 g) in the presence of a

catalytic amount of sodium ethoxide. Similar to CTWK-MAG, the coupling procedure of S-MAG to obtain WSCS-MAG was carried out.

WSCS-MAG: FTIR (KBr, ν cm^{-1}): 2937, and 2873 cm^{-1} (C-H stretching), 1655 and 1560 cm^{-1} (amide I and II), 569 cm^{-1} (Fe-O).

Scheme 4.1 Preparation of CTWK-MAG and WSCS-MAG.

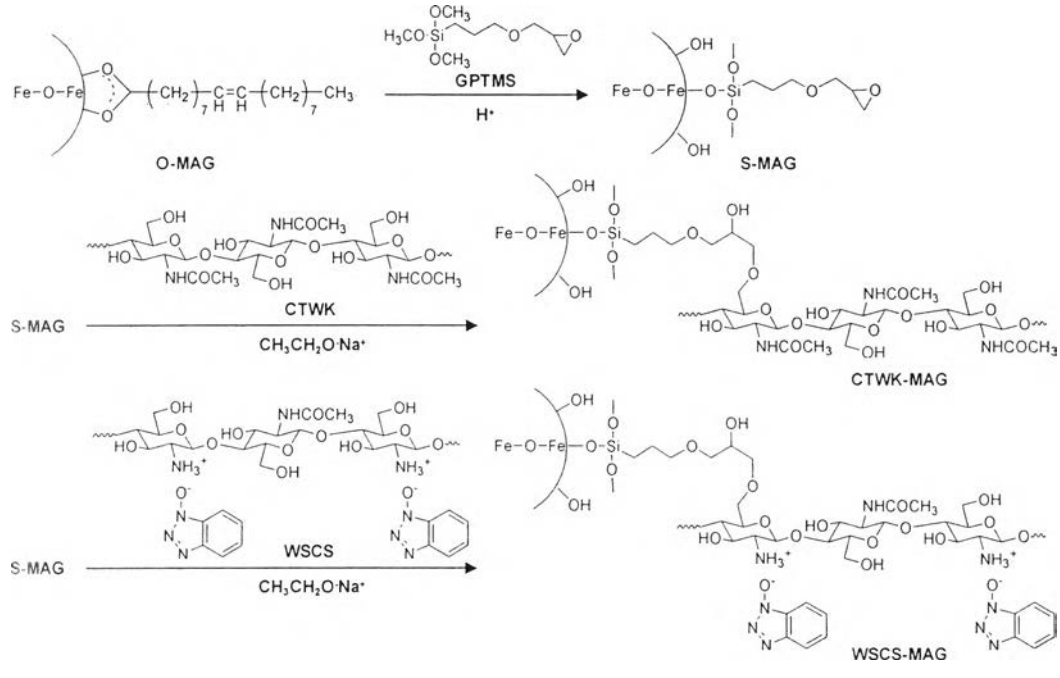

4.3.6 DNA Extraction from Bacterial Cells

Escherichia coli ATCC 25922 (*E. coli*) and *Staphylococcus aureus* ATCC 25923 (*S. aureus*) cells were grown in Luria–Bertani (LB) medium and the cell turbidity was adjusted using McFarland standard No. 0.5 (~1.5×10^8 cells/mL). For the extraction process, 200 μL of bacterial cell suspensions were added equally with alkaline lysis solution (0.2 M NaOH and 1%(w/v) sodium dodecyl sulfate). The contents in the microcentrifuge tube were gently mixed and incubated at room temperature for 5 min. After incubation, 50 μL of CTWK-MAG sample (10 mg/mL) was added followed by the addition of binding buffer (4 M NaI and 20%(w/v) polyethylene glycol 8000, 200 μL). The mixture was gently inversed and incubated at room temperature for 5 min. The CTWK-MAG were trapped by an external

magnet and the supernatant was removed. The trapped CTWK-MAG were washed two times with cold ethanol/water (70%w/w) and dried at room temperature for 5 min. The CTWK-MAG were then suspended in TE buffer (50 mM Tris-HCl, 1 mM EDTA, pH 8.0) and the bound DNA was eluted by incubation at 65 °C. After elution, the solution was transferred to a new microcentrifuge tube and stored at -20 °C until qualitatively analyzed. Similar procedures were carried out using WSCS-MAG.

4.3.7 Characterizations

Fourier transform infrared (FTIR) spectra were recorded by using a Thermo Nicolet Nexus 670 with 32 scans at a resolution of 2 cm^{-1} and a frequency range of 4000–400 cm^{-1}. The colloidal stability was evaluated by a Shimadzu UV-1800 spectrophotometer at a wavelength of 400 nm. Relative absorbance was calculated based on the absorbance at 400 nm at 15, 30, 60, 120 and 180 min after sonication, divided by the absorbance at the starting time, i.e. the time soon after sonication. The samples were dispersed in 5×10^{-5} g/mL solutions. Particle size and zeta potential were measured by a Malvern Zetasizer Nano ZS at 25 °C. Morphological studies were done by using a Hitachi transmission electron microscope H-7650 at an operating voltage of 100 kV. Thermal properties were investigated by a Perkin Elmer thermo gravimetric/differential thermal analyzer (TG/DTA) Pyris Diamond from 30 °C to 800 °C with a heating rate of 10 °C/min under nitrogen atmosphere. The nitrogen flow rate was 100 mL/min. The thermogravimetric analyzer interface with Fourier transform infrared spectroscopy (TG-FTIR) measurements was carried out by using a TA TGA-Q50 interface with a Thermo Nicolet Nexus 670 Fourier transform infrared spectrophotometer (FTIR, USA). The TG measurements were performed using a heating rate of 10 °C/min, from 30 °C to 600 °C, under nitrogen. Each spectrum was recorded by FTIR every 60 sec with a 4 cm^{-1} resolution. Surface area was determined based on Brunauer Emmett Teller (BET) by using an Autosorp-1 gas sorption system (Quantachrome Corporation). The samples were preheated in nitrogen for 3 h to 4 h at 100 °C before analysis.

4.4 Results and Discussion

4.4.1 Preparation and Characterization of WSCS-MAG and CTWK-MAG

In the first step, MAG was treated with oleic acid during co-precipitation to get O-MAG. The use of oleic acid to treat the surface of MAG was carried out following the procedure reported by De Palma (De Palma *et al.*, 2007) but using epoxy silane instead of amino, aldehyde, acrylate, isocyanate, thiol, poly(ethylene glycol), cyano, and carboxylic acid silanes. At this step, FTIR was used to follow the chemical modification. The MAG showed a strong characteristic peak of Fe-O at 573 cm^{-1} only, whereas O-MAG additionally showed C-H stretching at 2922 cm^{-1}, and 2851 cm^{-1}. An epoxy silane coupling agent, GPTMS was used to perform a ligand exchange with oleic acid-coated MAG in the presence of a catalytic amount of acetic acid. As shown in Figure 4.1A (a), characteristic peaks at 588 cm^{-1} (Fe-O), 900 cm^{-1} (oxirane ring), and 1087 cm^{-1} (Si-O) confirm the success of MAG surface modification with GPTMS. Figure 4.1A ((b) and (c)) show FTIR spectra of CTWK-MAG, and WSCS-MAG, respectively.

As the characteristic peak of Si-O stretching at ~1100 cm^{-1} overlaps the fingerprints of chitin and chitosan, curve fitting analysis was carried out for quantification. It has to be mentioned that after the reaction finished, uncoupled MAG soon precipitated. Consequently, the particles could be easily excluded from the colloidal solution by using a magnet before decanting the colloidal solution. Figure 4.1B shows the curve fittings of CTWK, and WSCS after coupling with S-MAG. It is clear that the decrease of the oxirane peak at 900 cm^{-1} significantly proves the successful coupling reaction via covalent bonding. It should be noted that in most cases, the coupling reaction between epoxy group and coating polymers were clarified based on analysis using FTIR spectra. Here, the coupling reaction was evaluated by using curve fitting FTIR technique and quantitatively analyzed by taking the ratio of specific peaks, i.e. 1100 cm^{-1} (Si-O peak) and 900 cm^{-1} (oxirane peak). As shown in Figure 4.1C, in the case of CTWK-MAG, the decrease of the integral peak ratio between the oxirane peak and Si-O peak is not as high as WSCS-MAG. The reactivity of CTWK might be a consequence of heterogeneous reaction condition.

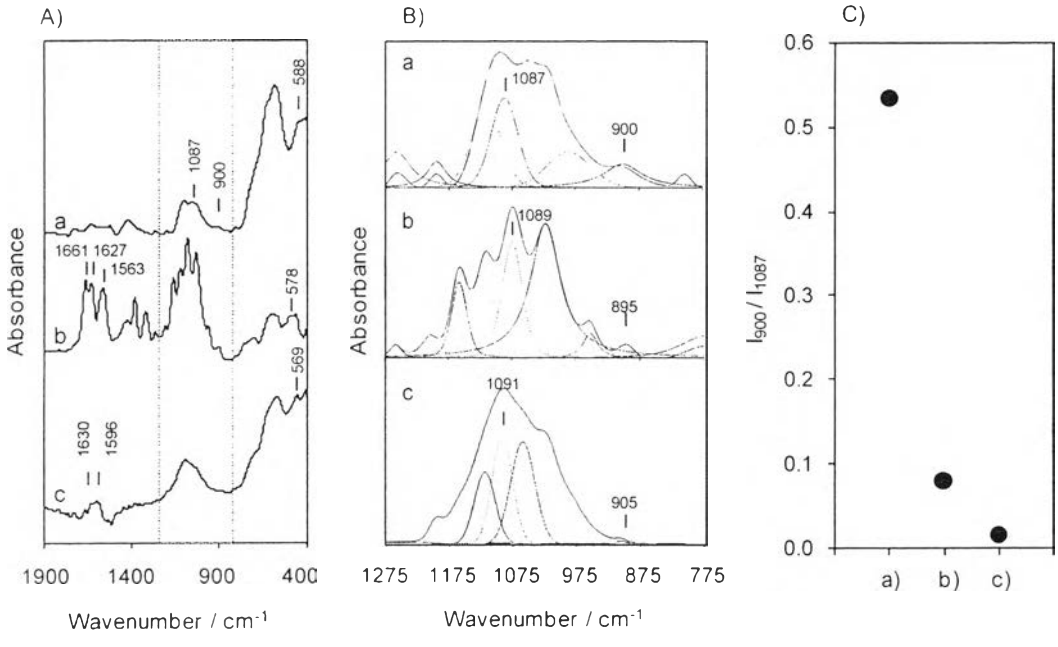

Figure 4.1 A) FTIR spectra of (a) S-MAG, (b) CTWK-MAG, and (c) WSCS-MAG; B) curve fitting of (a) S-MAG, (b) CTWK-MAG, and (c) WSCS-MAG; and C) integral ratio of oxirane peak at 900 cm^{-1} to Si-O peak at 1087 cm^{-1} of a) S-MAG, b) CTWK-MAG, and c) WSCS-MAG.

It comes to the question that the use of trialkoxy silane might bring the crosslink network between MAG and GPTMS. Considering the requirement of the covalent bond between MAG and CTWK or WSCS as an aim in this work, the use of trialkoxy silane nevertheless satisfies the condition. At the present, the comparative study using mono- and di-alkoxy silane is under progress.

In this work, a structural characterization by NMR technique could not be done due to the ferrous oxide magnetization. Therefore, thermogravimetric analysis (TGA) was carried out as an indirect method to confirm the success of the coupling reaction and to quantitatively study the chemical composition. In order to make the evaluation proper in all cases, the TGA analysis were done three times and the ash content was determined at 500 °C where CTWK and WSCS were completely degraded. Basic information relating to this analysis is (i) MAG showed no degradation up to 800 °C; (ii) CTWK and WSCS were thermally degraded at ~400 °C, and ~250 °C with the ash content of 30.2%, and 39.5%, respectively; and (iii)

oleic acid and GPTMS degraded almost completely at the temperature above 400 °C with only few percent of ash content.

In the case of O-MAG (Figure 4.2 (a)), there are two weight losses in total (31.4%) appearing at 253 °C and 351 °C. This suggests the covering of oleic on MAG as bi-layer as reported by Shen *et al.* (Shen *et al.*, 1999). In addition, TGA-FTIR of O-MAG shows only C-H stretching peaks at 2850 cm^{-1}–2920 cm^{-1} confirming the degradation of oleic acid during thermal treatment. The TGA of O-MAG also reveals a peak at 773 °C referring to the Currie temperature of ferrous oxide.

For S-MAG (Figure 4.2 (b)), the degradation temperatures shift to 213 °C and to 420 °C. At that time, the ash contents of GPTMS and MAG are 12.4%, and 86.5%, respectively. It should be noted that oleic acid completely degraded and no ash content appeared above 400 °C but GPTMS showed the ash content of 5.7% (see the Supporting Information, Figure S2 (b) and (c)). Therefore, the weight loss at about 500 °C can be assigned to MAG on the condition that the ash content of GPTMS as low as 5.7% was neglected.

For CTWK-MAG (Figure 4.2 (c)), the weight loss of CTWK is as high as 61.4%. By using the DTG peak to identify the position of degradation temperature, it is clear that the degradation temperature of CTWK in CTWK-MAG is at 369 °C which is lower than that of the pure CTWK (380 °C) (see the Supporting Information, Figure S2 (d)). This implies the loose packing of CTWK as a consequence of the coupling to MAG.

In the case of WSCS-MAG (Figure 4.2 (d)), the degradation peaks are identified at 281 °C and 388 °C. As compared to the degradation of pure WSCS at 244 °C, the shift of the degradation temperature implies that WSCS was successfully coupled to MAG. Based on the ash content of 30.2% for CTWK, and 36.7% for WSCS, the MAG content for CTWK-MAG, and WSCS-MAG can be calculated as 2.4%, and 70.1%, respectively.

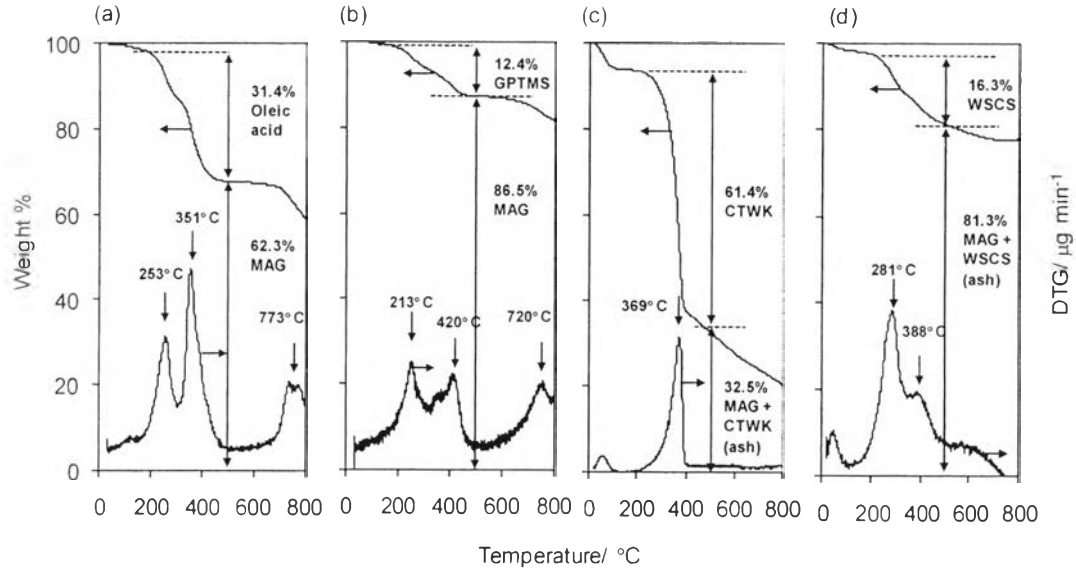

Figure 4.2 TGA thermograms of (a) O-MAG, (b) S-MAG, (c) CTWK-MAG, and (d) WSCS-MAG.

4.4.2 Morphologies of WSCS- MAG and CTWK-MAG

Transmission electron microscopy (TEM) was used to observe changes in MAG after modification. Figure 4.3 (a) shows a TEM image of freshly prepared MAG having an average diameter of ~15 nm. It should be noted that MAG particles are aggregated at a certain level. However, after modification to O-MAG, the particles (Figure 4.3 (b)) are well dispersed with an individual particle size of ~5 nm to 20 nm (average size ~10 nm). Figure 4.3 (c) shows a uniform whisker which is similar in dimension to the literature (Phongying *et al.*, 2007). In the case of WSCS (Figure 4.3 (d)), the particles appear in cluster form.

Figures 4.3 (e) and (f) show the presence of MAG, identified by the dark spots. CTWK-MAG (Figure 4.3 (e)) shows a uniform whisker of CTWK-MAG evenly dispersed on the TEM image. WSCS-MAG (Figure 4.3 (f)) reveals the existence of MAG (size ~50–500 nm) in fibrous clusters.

As CTWK shows whisker or needle-like morphology, a regular packing of the liquid crystalline state can be assumed (Lin *et al.*, 2012). We questioned whether the magnetic field is able to direct an alignment of CTWK-MAG or not. A simple trial to develop the CTWK-MAG alignment was done by placing a

copper grid spread with CTWK-MAG between two strong magnets followed by air-drying. Figure 4.3 (g) shows TEM micrographs where a bunch of CTWK-MAG aligned in the same direction, which is completely different from the randomly aligned CTWK-MAG without magnetic field. This indicates an advantage of chitosan in whisker form, especially when a regular alignment of magnetic particles or a specific morphology is needed.

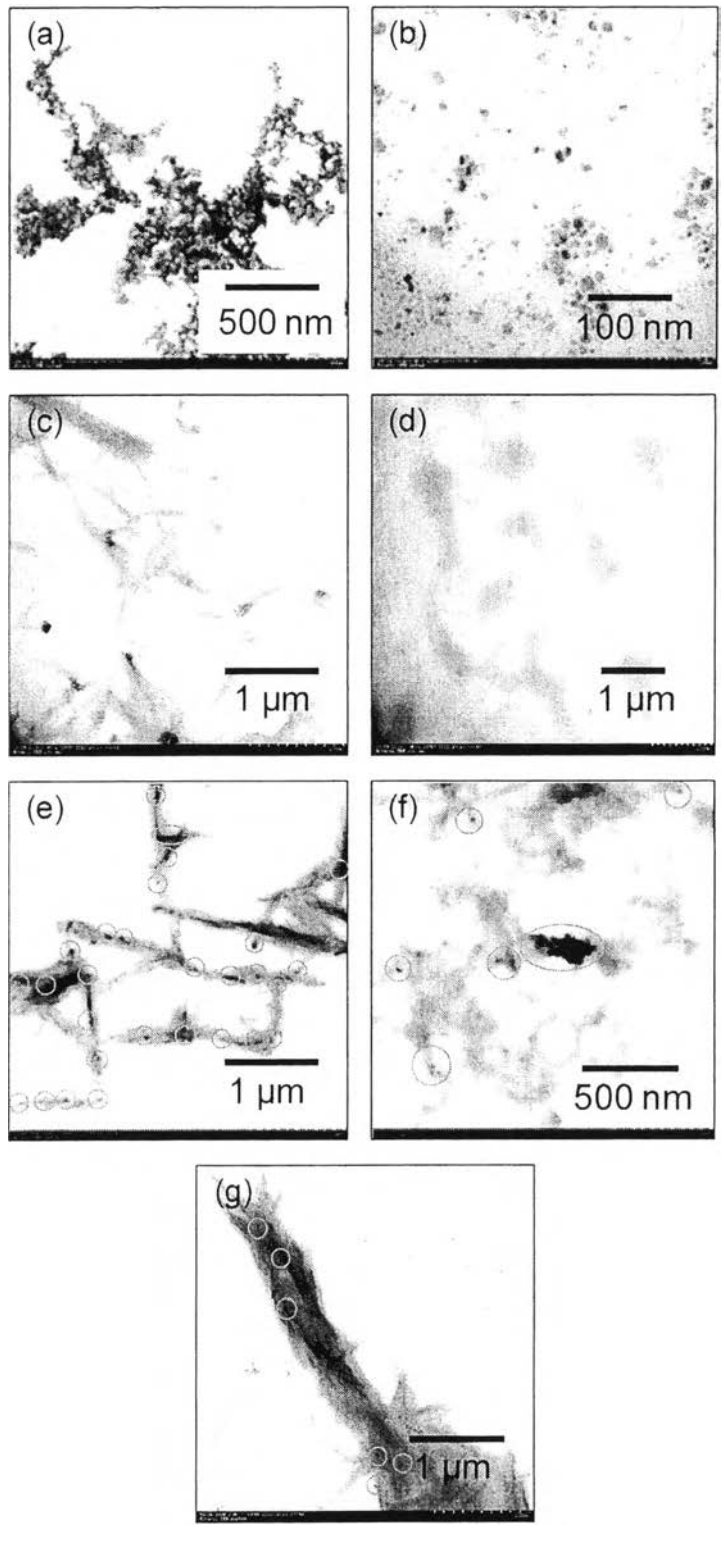

Figure 4.3 TEM micrographs of (a) MAG, (b) O-MAG, (c) CTWK, (d) WSCS, (e) CTWK-MAG, (f) WSCS-MAG, and (g) CTWK-MAG under magnetic field. Circles in Figure (e-g) indicate MAG.

4.4.3 Stability of WSCS-MAG and CTWK-MAG in Aqueous Solution

Colloidal stability is one of the most important requirements of MAG-based material, especially for bio-related applications. The colloidal stability of CTWK-MAG and WSCS-MAG in water in comparison to MAG and S-MAG was initially evaluated by appearance (Figure 4.4A). With MAG and S-MAG (Figure 4.4A (a) and (b)), the cloudy solution becomes clear after 60 min. In fact, the precipitation started within the first 15 min. This reflects the poor stability of MAG and S-MAG in water. In the case of WSCS-MAG (Figure 4.4A (d)), the solution maintained its colloidal state with only slight aggregation after 60 min. The colloidal stability becomes more significant for CTWK-MAG (Figure 4.4A (c)) as evidenced by the colloidal state after 180 min.

Quantitative analyses of the colloidal stability of MAG, S-MAG, CTWK-MAG, and WSCS-MAG were further carried out (Figure 4.4B) by measuring the absorbance at 400 nm at each time intervals. The normalization was calculated from the absorbance of the colloidal solution at a specific time divided by the absorbance soon after sonication. For MAG and S-MAG, a significant decrease in the relative absorbance is observed soon after the solution was left standing. In contrast, the relative absorbance of CTWK-MAG remains constant even after 180 min. This finding indicates excellent colloidal stability of CTWK-MAG in water. This behavior might be due to the CTWK-MAG particles, which are entangled, leading to prolonged dispersibility. In the case of WSCS-MAG, the relative absorbance drops to 0.86 after 15 min and continues decreasing. This result might be related to the aggregation of WSCS as the hydrogen bond formation among WSCS or on the MAG hydrophilic surface is more favored.

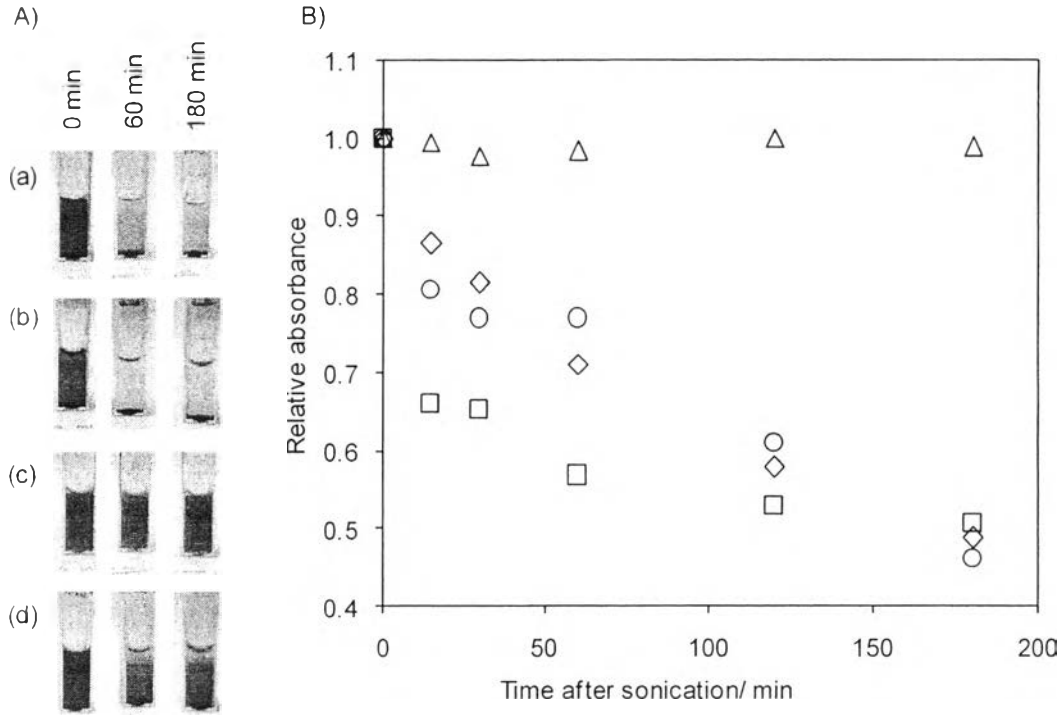

Figure 4.4 A) Photographs of colloidal appearances of (a) MAG, (b) S-MAG, (c) CTWK-MAG, and (d) WSCS-MAG; and B) relative absorbance of MAG (○), S-MAG (□), CTWK-MAG (△), and WSCS-MAG (◇) in water as a function of time.

4.4.4 CTWK-MAG under Solvent Effect

To investigate how colloidal stability is influenced by the solvent polarity, CTWK-MAG was dispersed in several polar as well as nonpolar solvents. The concentration of CTWK-MAG was prepared in high concentration in order to follow the changes in colloidal stability easily. CTWK-MAG showed long-term stability in water. In relation to the dielectric constant (k), (Dean, 1999) the solvents were chosen in the order of water (k=80.1), DMSO (k=46.7), methanol (k=32.7), ethanol (k=24.5), DMF (k=19.9), THF (k=7.58), chloroform (k=4.81), and toluene (k=2.38). Figure 4.5A shows the colloidal appearances. In all conditions, CTWK-MAG shows good dispersibility soon after shaking and sonication (t_0 min). The colloidal stability is maintained, only in the cases of water and DMSO, for 180 min while rapid precipitation can be observed after 15 min, especially for methanol and

ethanol. The precipitation is more distinct in DMF, THF, chloroform, and toluene. It is important to note that no MAG separation occurs in any solvent. This indicates a non hydrolysable covalent bond between CTWK and MAG.

In order to quantify colloidal stability, relative visible absorbance was measured. Among all solvents used, CTWK-MAG shows the highest, nearly constant value in water (Figure 4.5B). For methanol and ethanol, which are classified as protic solvents, the relative absorbance decreases significantly at about 0.4. The aggregation of CTWK-MAG might be due to the formation of hydrogen bonds in each particle.

In the cases of aprotic polar solvent, CTWK-MAG shows a slight decrease in absolute absorbance to 0.8 in DMSO, whereas other aprotic polar solvents (DMF and THF) display a drastic decreased value. A reason for this could be that the interaction between CTWK-MAG and DMSO might be related to the dipole moment (3.96 D). With the aprotic non-polar solvent (toluene), it is clear that CTWK-MAG quickly precipitated. Similar to this, chloroform, which is aprotic but polar, the hydrogen bond network in CTWK might have been enhanced until CTWK-MAG precipitated out of the system. It is important to note that the photograph (Figure 4.5A) and the plot (Figure 4.5B) confirm us for the first time about the solvent responsiveness of CTWK-MAG under variation of solvent polarity.

Figure 4.5C (a) to (c) illustrates possible interactions based on the results in Figure 4.5B. The interaction of CTWK-MAG with solvents is related to the formation of a hydrogen bond network between the OH or NH_2 groups of CTWK and the OH group at the MAG surface. Additionally, the interaction is supported by the polarity of MAG.

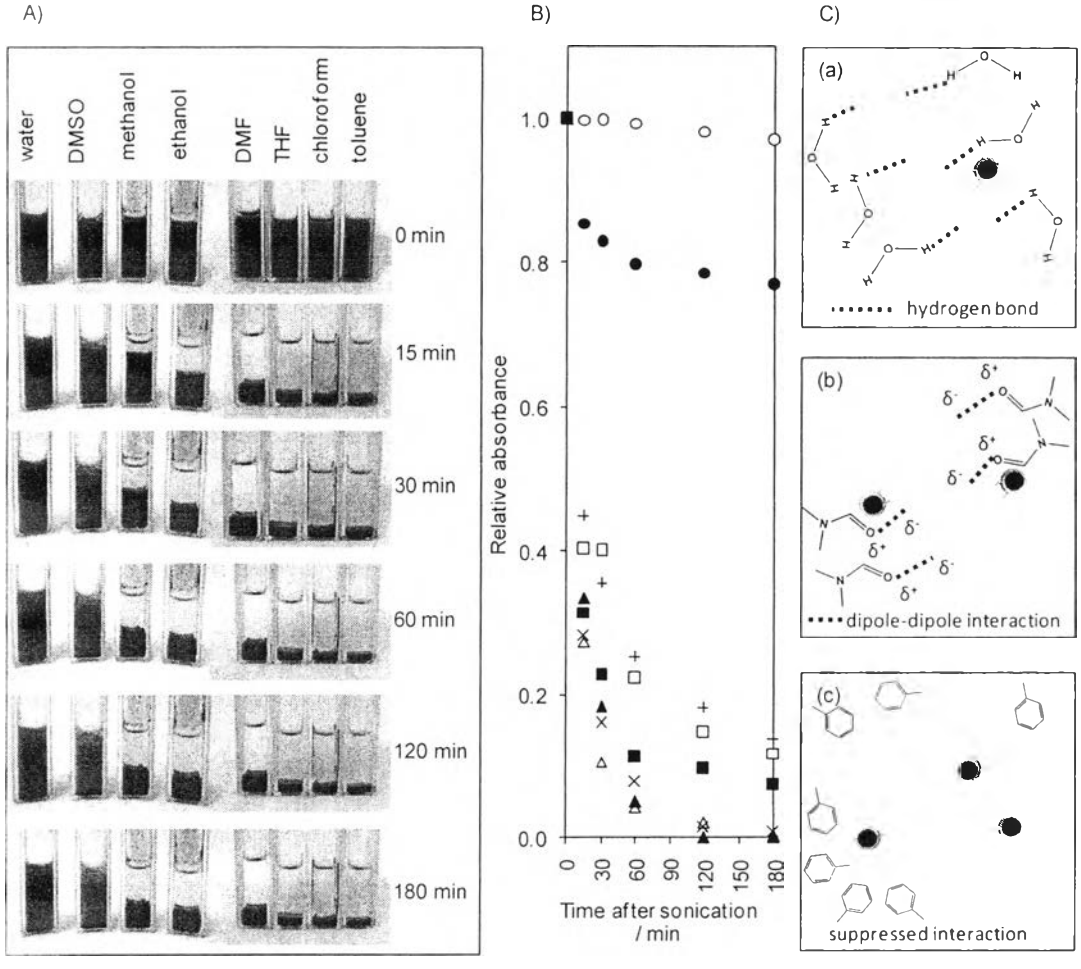

Figure 4.5 A) Photographs of CTWK-MAG dispersed in various solvents in relation to the dielectric constant value (k): toluene (k=2.38), chloroform (k=4.81), THF (k=7.58), DMF (k=19.9), ethanol (k=24.5), methanol (k=32.7), DMSO (k=46.7), and water (k=80.1) at 0 min, 30 min, 60 min, 120 min, and 180 min after sonication; B) relative absorbance of CTWK-MAG in various solvents: water (○), DMSO (●), methanol (□), ethanol (■), DMF (△), THF (▲), chloroform (+), and toluene (×); and C) schematic illustration of solvent interactions to CTWK-MAG in (a) water, (b) DMF, and (c) toluene.

4.4.5 Surface Properties and Particle Size Related to pH

The size of the particle was traced by DLS under various pH levels. It should be noted that DLS measures particle size in the solution state. The relationship between the zeta potential and particle size as a function of pH are

depicted in Figure 4.6A., The zeta potential is highly positive (~over 30 mV) from pH 2 to pH 5 and highly negative (~-40 mV) from pH 8 to pH 10 for MAG (Figure 4.6A (a)), while at pH 6 to pH 7 the charge is almost at zero. The particle size of MAG is as high as 3000 nm to 4000 nm. This indicates the aggregation in all pH range as a consequence of an ease of hydrogen bond formation between each particle.

The zeta potential values of S-MAG tend to be negative (as high as ~-40 mV) in most conditions except at pH 2–3 which is ~+5 mV (Figure 4.6A (b)). The sizes (~800 nm–2000 nm) over the whole pH range are much lower than that of MAG (1000 nm–4000 nm). This reflects the coverage of silane on MAG leading to a suppressed hydrogen bond network.

It becomes clear that the size and the charge reveal a relationship, the higher the charge of CTWK-MAG, the smaller the particle size (Figure 4.6A (c)). For example, when CTWK-MAG carries a positive charge from 20 mV to 40 mV at pH 2–4, the average size is less than 1000 nm. The size of CTWK-MAG in dependence to the pH is quite different from that of CTWK. For CTWK, the size is almost maintained at a few hundred nanometers from acidic pH to neutral pH, and it is significantly increased to sub-micrometers (3000 nm–7000 nm) in basic pH. This means that the MAG coupling, consequently, changed pH responsiveness of CTWK.

In order to summarize the overall results, a schematic representation for CTWK-MAG and WSCS-MAG at different pH conditions is illustrated (Figure 4.6B). Figure 4.6B (a) is for CTWK-MAG at low pH when CTWK are protonated according to the positive zeta potential values. Therefore, CTWK-MAG repulse each other leading to the smaller sizes. At neutral pH condition (Figure 4.6B (b)), a certain level of positive charge with a minor repulsive force, causes an increase of particle size. At the same time the hydrogen bonds (represented as a dashed line) among the whiskers become significant resulting in an increase in size. At alkaline condition, the zeta potential values are slightly negative but the particles become larger. This leads us to the conclusion that CTWK forms a packed structure induced by a strong hydrogen bond network on the surfaces of CTWK (Figure 4.6B (c)). This schematic drawing show that the sizes of CTWK-MAG in alkaline condition are significantly increased compared to those of CTWK.

In our previous work, the structure of WSCS under the complexation with HOBt was clarified. It becomes clear that solubility in water is based on the effect of HOBt functioning as a proton donor to form ammonium groups within the chitosan chain. Based on this information, the hydrogen bonds along the WSCS chains might be maintained by HOBt resulting in the particle sizes about 2000 nm - 3000 nm (WSCS-MAG at acidic pH). The zeta potential, therefore, depends on the protonated WSCS-MAG surface (Figure 4.6C (a)). At neutral pH, WSCS-MAG exhibits almost no significant changes at the surface as shown in Figure 4.6C (b). This suggests the hydrogen bonds between each particle. At alkaline condition (Figure 4.6C (c)), although the negative charges cover WSCS-MAG and complexation between HOBt and WSCS is maintained, a constant particle size of WSCS-MAG (at ~1500 nm–2500 nm) is still observed.

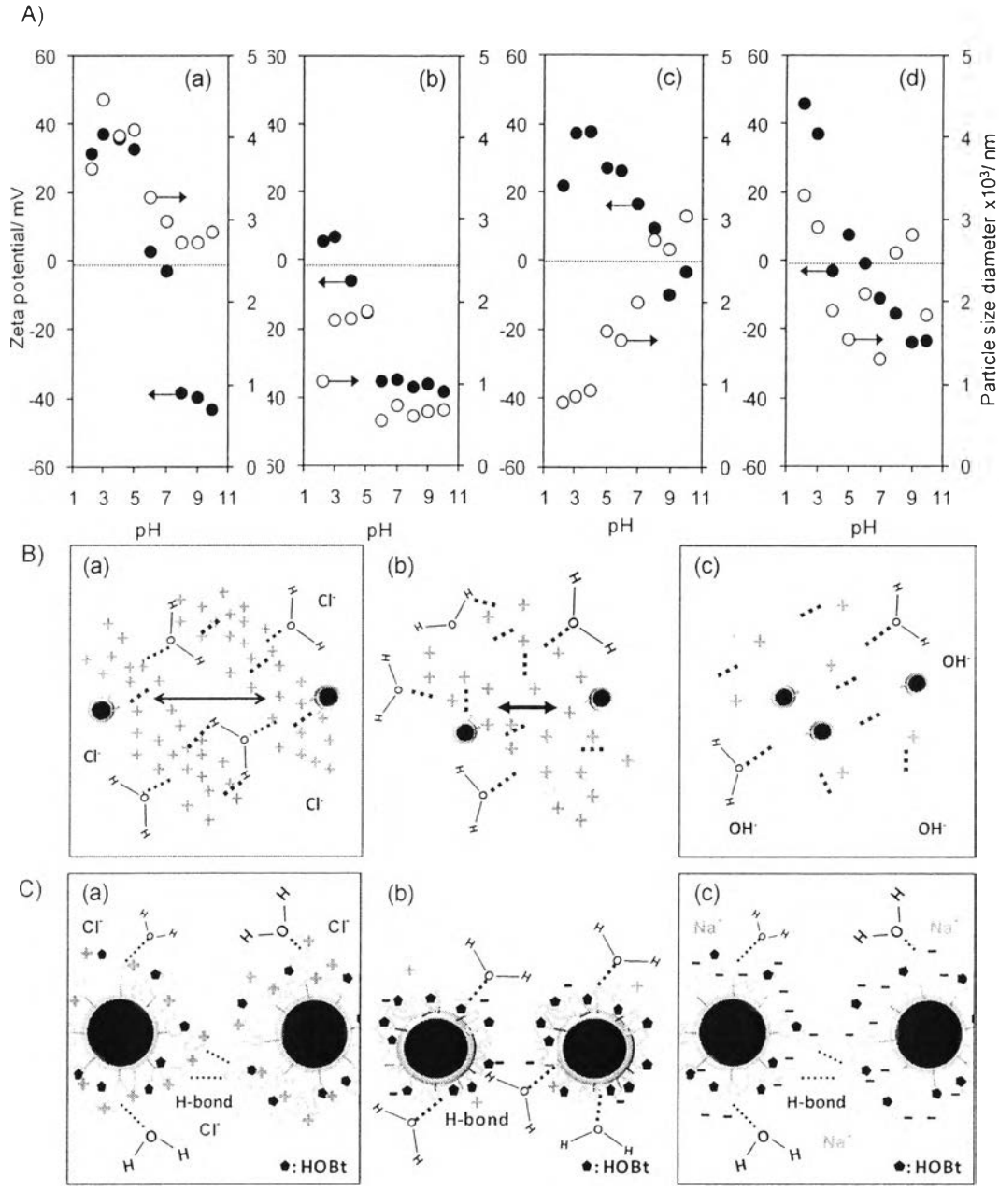

Figure 4.6. A) Zeta potential and particle size of (a) MAG, (b) S-MAG, (c) CTWK-MAG, and (d) WSCS-MAG at pH 2.2 to pH 10 in water (pH adjusting by NaOH and HCl); B) schematic illustrations of CTWK-MAG in water at (a) pH 2–4, (b) pH 5–7, and (c) pH 8–10; and C) schematic illustrations of WSCS-MAG in water at (a) pH 2–3, (b) pH 3–7, and (c) pH 8–10.

4.4.6 Performances of WSCS-MAG and CTWK-MAG for Bacterial DNA Extraction

In order to investigate potential for application of WSCS-MAG and CTWK-MAG, a preliminary examination on bacterial DNA extraction was carried out. The study on DNA extraction leads us to the information about the integrated properties of the MAG compounds, especially the interaction with biomolecules. It is important to note that, the efficiency of MAG for DNA separation is related to the physical properties in terms of surface area and stability in solution, in order to enable an effective interaction between MAG and DNA. However, to obtain specific interaction between DNA and MAG at the molecular level, a highly selective MAG material is required. As chitosan is an aminopolysaccharide, interactions between chitosan and DNA, either mediated by the positively charged chitosan and negatively charged DNA or by a hydrogen bond network. Moreover, CTWK-MAG and WSCS-MAG also showed a superparamagnetic property.

The amounts of DNA extracted from *E.coli* and *S.aureus* are presented in Table 4.1. WSCS-MAG shows 100% more extracted DNA (10.89 μg/mL) than CTWK-MAG for *E.coli*. This confirms the significant DNA extraction property of WSCS-MAG. When using *S.aureus*, CTWK-MAG and WSCS-MAG show almost equal amounts. In order to compare the efficiency of CTWK-MAG and WSCS-MAG, a commercially available magnetic kit was applied. The extracted DNA was ~4.54 ± 0.8 μg/mL for *E.coli* and ~2.87 ± 1.5 μg/mL for *S.aureus*. In comparison, the result of our material, especially the higher extraction amount for WSCS-MAG, implies the essential role of chitosan. Thereby improved extraction is might be related to ionic interactions of the ammonium groups of CS and the negatively charged cell walls of bacteria.

Furthermore, the surface area is an indicator that reflects the effectiveness of the materials, since the size of the active surface is responsible for the interaction of MAG with DNA species. The surface area of the commercial products is ~1–10 m^2/g whereas CTWK-MAG and WSCS-MAG are ~82.32 m^2/g and 44.76 m^2/g, respectively. The significantly increased active surface area suggests the potential applicability of our new materials.

4.5 Conclusions

Two types of chitin and chitosan materials, CTWK (chitin in whisker form) and WSCS (chitosan in water soluble form), were successfully covalently bonded to MAG. Because of the silane coupling agent containing oxirane ring, a single-step procedure to couple chitosan to MAG without any additional steps during the conjugating reaction was possible. The fibrous chitin whisker (CTWK) was effectively coupled to MAG resulting in a stable colloidal solution. The irregular packing of CTWK led to a significant aqueous colloidal stability for days. The uniqueness of CTWK-MAG was also related to the whisker morphology as a magnetic field effectively induced a CTWK-MAG alignment. The ionic charge of CTWK, which could be varied by pH, was a key factor to control the size of CTWK-MAG. WSCS is a water-soluble chitosan in complexation with HOBt. In the case of WSCS-MAG, the surface of MAG was partially covered resulting in aggregation over time based on a hydrogen bond network among chitosan chains and HOBt. The preliminary examination results of *E.coli* and *S.aureus* DNA extraction confirmed the performance of CTWK-MAG and WSCS-MAG for DNA separation.

4.6 Acknowledgements

This work was supported by the National Nanotechnology Center (NANOTEC), the National Science and Technology Development Agency (NSTDA), Thailand (Project No. NN-B-22-FN1-10-52-14). One of the authors (S. Chatrabhuti) thanks the Center for Petroleum, Petrochemical and Advanced Materials, and the Petroleum and Petrochemical College, Chulalongkorn University for the Ph.D. scholarship. The supports by the National Research Council of Thailand (NRCT) and Integrated Innovation Academic Center: IIAC Chulalongkorn University Centenary Academic Development Project are gratefully acknowledged. Chitosan was kindly supplied by Seafresh Chitosan (Lab) Company Limited, Thailand and Chitin Research Center, Chulalongkorn University. Gratitude is also extended to Hitachi High Technologies for the TEM measurement, and to Dr. Pongsakorn Chantarat, Department of Physics, Kasetsart University, for the

magnetization measurement. The authors thank Dr. Surachai Ngamratanapaiboon, Department of Biochemistry, Faculty of Pharmacy, Mahidol University for his help on the DNA extraction study.

4.7 References

Bica, D., Vékás, L., Avdeev, M. V., Marinică, O., Socoliuc, V., Bălăsoiu, M. and Garamus, V. M. (2007) Sterically Stabilized Water Based Magnetic Fuids: Synthesis, Structure and Properties. Journal of Magnetism and Magnetic Materials, 311(1), 17-21.

De Palma, R., Peeters, S., Van Bael, M. J., Van den Rul, H., Bonroy, K., Laureyn, W., Mullens, J., Borghs, G. and Maes, G. (2007) Silane Ligand Exchange to Make Hydrophobic Superparamagnetic Nanoparticles Water-Dispersible. Chemistry of Materials, 19(7), 1821-1831.

Fangkangwanwong, J., Akashi, M., Kida, T. and Chirachanchai, S. (2006) Chitosan-Hydroxybenzotriazole Aqueous Solution: A Novel Water-Based System for Chitosan Functionalization. Macromolecular Rapid Communications, 27(13), 1039-1046.

Gelbrich, T., Feyen, M. and Schmidt, A. (2006) Magnetic Thermoresponsive Core-Shell Nanoparticles. Macromolecules, 39(9), 3469-3472.

Gupta, A. K. and Gupta, M. (2005) Synthesis and surface engineering of iron oxide nanoparticles for biomedical applications. Biomaterials, 26(18), 3995-4021.

Hu, J., Yin, L. and Jia, L. (2011) Chitosan–silica hybrid-coated open tubular column for hydrophilic interaction capillary electrochromatography. Journal of Separation Science, 34(5), 565-573.

Hu, X., Tang, Y., Wang, Q., Li, Y., Yang, J., Du, Y. and Kennedy, J. F. (2011) Rheological behaviour of chitin in NaOH/urea aqueous solution. Carbohydrate Polymers, 83(3), 1128-1133.

Jing, Z. and Wu, S. (2004) Synthesis and characterization of monodisperse hematite nanoparticles modified by surfactants via hydrothermal approach. Materials Letters, 58(27–28), 3637-3640.

Kim, S. Y., Ramaraj, B. and Yoon, K. R. (2012) Preparation and characterization of polyvinyl alcohol-grafted Fe3O4 magnetic nanoparticles through glutaraldehyde. Surface and Interface Analysis, 44(9), 1238-1242.

Lao, L. L. and Ramanujan, R. V. (2004) Magnetic and hydrogel composite materials for hyperthermia applications. Journal of Materials Science: Materials in Medicine, 15(10), 1061-1064.

Lin, N., Huang, J. and Dufresne, A. (2012) Preparation, properties and applications of polysaccharide nanocrystals in advanced functional nanomaterials: a review. Nanoscale, 4(11), 3274-3294.

Loo, A., Pineda, M., Saade, H., Treviño, M. and López, R. (2008) Synthesis of magnetic nanoparticles in bicontinuous microemulsions. Effect of surfactant concentration. Journal of Materials Science, 43(10), 3649-3654.

Lopez-Cruz, A., Barrera, C., Calero-DdelC, V. L. and Rinaldi, C. (2009) Water dispersible iron oxide nanoparticles coated with covalently linked chitosan. Journal of Materials Chemistry, 19(37), 6870-6876.

Moeser, G. D., Roach, K. A., Green, W. H., Laibinis, P. E. and Hatton, T. A. (2002) Water-Based Magnetic Fluids as Extractants for Synthetic Organic Compounds. Industrial & Engineering Chemistry Research, 41(19), 4739-4749.

Muzzarelli, R. A. A., Boudrant, J., Meyer, D., Manno, N., DeMarchis, M. and Paoletti, M. G. (2012) Current views on fungal chitin/chitosan, human chitinases, food preservation, glucans, pectins and inulin: A tribute to Henri Braconnot, precursor of the carbohydrate polymers science, on the chitin bicentennial. Carbohydrate Polymers, 87(2), 995-1012.

Phongying, S., Aiba, S.-i. and Chirachanchai, S. (2007) Direct chitosan nanoscaffold formation via chitin whiskers. Polymer, 48(1), 393-400.

Richardson, S. W., Kolbe, H. J. and Duncan, R. (1999) Potential of low molecular mass chitosan as a DNA delivery system: biocompatibility, body distribution and ability to complex and protect DNA. International Journal of Pharmaceutics, 178(2), 231-243.

Scarberry, K. E., Dickerson, E. B., McDonald, J. F. and Zhang, Z. J. (2008) Magnetic Nanoparticle−Peptide Conjugates for in Vitro and in Vivo

Targeting and Extraction of Cancer Cells. Journal of the American Chemical Society, 130(31), 10258-10262.

Shen, L., Laibinis, P. E. and Hatton, T. A. (1999) Bilayer Surfactant Stabilized Magnetic Fluids: Synthesis and Interactions at Interfaces. Langmuir, 15(2), 447-453.

Tadmor, R., Rosensweig, R. E., Frey, J. and Klein, J. (2000) Resolving the Puzzle of Ferrofluid Dispersants. Langmuir, 16(24), 9117-9120.

Xia, J., Liao, P. and Zhenyuan, N. (2006) Preparation and characterization of magnetic carboxymethylated chitosan-Fe_3O_4 nanocomposites for isolation of genomic DNA. Journal of Central South University(Science and Technology), 37(6), 1075-1080.

Xie, J., Chen, K., Lee, H.-Y., Xu, C., Hsu, A. R., Peng, S., Chen, X. and Sun, S. (2008) Ultrasmall c(RGDyK)-Coated Fe3O4 Nanoparticles and Their Specific Targeting to Integrin αvβ3-Rich Tumor Cells. Journal of the American Chemical Society, 130(24), 7542-7543.

Zargar, B., Parham, H. and Hatamie, A. (2009) Modified iron oxide nanoparticles as solid phase extractor for spectrophotometeric determination and separation of basic fuchsin. Talanta, 77(4), 1328-1331.

Zhang, J. L., Srivastava, R. S. and Misra, R. D. K. (2007) Core−Shell Magnetite Nanoparticles Surface Encapsulated with Smart Stimuli-Responsive Polymer: Synthesis, Characterization, and LCST of Viable Drug-Targeting Delivery System. Langmuir, 23(11), 6342-6351.